AAC Journals.ASM.org

Structural Insights into the Subclass B3 Metallo-β-Lactamase SMB-1 and the Mode of Inhibition by the Common Metallo-β-Lactamase Inhibitor Mercaptoacetate

Jun-ichi Wachino,[a,b] Yoshihiro Yamaguchi,[c] Shigetarou Mori,[a] Hiromasa Kurosaki,[d] Yoshichika Arakawa,[a,b] Keigo Shibayama[a]

Department of Bacteriology II, National Institute of Infectious Diseases, Musashi-Murayama, Tokyo, Japan[a]; Department of Bacteriology, Nagoya University Graduate School of Medicine, Showa-ku, Nagoya, Aichi, Japan[b]; Environmental Safety Center, Kumamoto University, Chuo-ku, Kumamoto, Japan[c]; Department of Structure-Function Physical Chemistry, Graduate School of Pharmaceutical Sciences, Kumamoto University, Chuo-ku, Kumamoto, Japan[d]

A novel subclass B3 metallo-β-lactamase (MBL), SMB-1, recently identified from a *Serratia marcescens* clinical isolate, showed a higher hydrolytic activity against a wide range of β-lactams than did the other subclass B3 MBLs, i.e., BJP-1 and FEZ-1, from environmental bacteria. To identify the mechanism underlying the differences in substrate specificity among the subclass B3 MBLs, we determined the structure of SMB-1, using 1.6-Å diffraction data. Consequently, we found that SMB-1 reserves a space in the active site to accommodate β-lactam, even with a bulky R1 side chain, due to a loss of amino acid residues corresponding to F31 and L226 of BJP-1, which protrude into the active site to prevent β-lactam from binding. The protein also possesses a unique amino acid residue, Q157, which probably plays a role in recognition of β-lactams via the hydrogen bond interaction, which is missing in BJP-1 and FEZ-1, whose K_m values for β-lactams are particularly high. In addition, we determined the mercaptoacetate (MCR)-complexed SMB-1 structure and revealed the mode of its inhibition by MCR: the thiolate group bridges to two zinc ions (Zn1 and Zn2). One of the carboxylate oxygen atoms of MCR makes contact with Zn2 and Ser221, and the other makes contact with T223 and a water molecule. Our results demonstrate the possibility that MCR could be a potent inhibitor for subclass B3 MBLs and that the screening technique using MCR as an inhibitor would be effective for detecting subclass B3 MBL producers.

The emergence of β-lactamases capable of hydrolyzing carbapenem antibiotics, i.e., carbapenemases, is of substantial concern in clinical settings since carbapenem is an important tool for the treatment of infectious diseases caused by pathogenic Gram-negative bacteria (GNB) (1). Metallo-β-lactamase (MBL; class B β-lactamase) is one of the prevalent carbapenemases among the pathogenic GNB. MBLs commonly contain one or two zinc ions in the active site and are further subdivided into three subclasses—B1, B2, and B3—based on their primary zinc binding motifs (2).

To date, a variety of MBL genes have been discovered on the chromosomes of human opportunistic and environmental bacteria, for example, L1 from *Stenotrophomonas maltophilia* (3), IND from *Chryseobacterium indologenes* (4), Sfh-1 from *Serratia fonticola* (5), CcrA from *Bacteroides fragilis* (6), CAU-1 from *Caulobacter crescentus* (7), and BJP-1 from *Bradyrhizobium japonicum* (8). On the other hand, horizontally acquired MBL genes, such as bla_{IMP} (9), bla_{VIM} (10), bla_{NDM} (11), bla_{SPM} (12), bla_{GIM} (13), and bla_{SIM} (14), have mainly been found on the plasmids of members of the family *Enterobacteriaceae*, *Pseudomonas* spp., and *Acinetobacter* spp.

We recently identified a novel subclass B3 MBL, named SMB-1, from a human opportunistic bacterium, *Serratia marcescens*, which was isolated from the urine of an inpatient in a Japanese hospital (15). SMB-1 can hydrolyze a variety of β-lactam antibiotics, including penicillins, cephalosporins, and carbapenems, as efficiently as the other subclass B3 MBLs, L1, and GOB-1 of *Elizabethkingia meningoseptica* (16, 17). On the other hand, despite belonging to the same subclass B3 MBL group, the enzymes BJP-1, CAU-1, THIN-B (of *Janthinobacterium lividum*), and FEZ-1 (of *Fluoribacter gormanii*) from environmental bacteria, have high K_m values for various β-lactams, resulting in very low affinities for the substrates and thus low catalytic efficiency (k_{cat}/K_m) (7, 8, 18, 19). There is a significant difference in hydrolytic activity against β-lactams between subclass B3 MBLs from human opportunistic bacteria and those from environmental bacteria.

Most of the subclass B3 MBL genes identified thus far were intrinsically located on the chromosomes of human opportunistic and environmental bacteria (3, 7, 8), whereas two subclass B3 MBLs, SMB-1 and AIM-1, which are predicted to be incorporated into pathogenic bacteria via mobile genetic element, were reported quite recently (15, 20). The SMB-1 gene was hypothesized to have been incorporated into the chromosome of the *S. marcescens* strain from an unknown bacterial species, via an IS*CR1* element, which was previously identified to be involved in the dissemination of a variety of antibiotic resistance genes (15, 21). These indicate the possibility that not only subclass B1 MBLs, such as IMP-type, VIM-type, and NDM-type MBLs, but also subclass B3 MBLs, such as SMB-1 and AIM-1, could become widely distributed among pathogenic bacteria, resulting in a serious clinical threat.

Many techniques of screening for MBL producers are available in routine clinical microbiology settings; however, the application

Received 18 June 2012 **Returned for modification** 11 August 2012
Accepted 7 October 2012
Published ahead of print 15 October 2012
Address correspondence to Jun-ichi Wachino, wachino@nih.go.jp.

doi:10.1128/AAC.01264-12

of these techniques has been evaluated mainly for subclass B1 MBL producers and has not been fully evaluated for subclass B3 MBL producers. In Japan, a phenotypic method, based on a β-lactam–sodium mercaptoacetate (MCR) synergy test, is frequently used for detecting MBL producers (22, 23). We previously reported that this synergy test showed a positive result for the SMB-1-producing strain (15), but its mode of inhibition remained unknown.

In order to understand the mechanism underlying substrate preferences observed among the subclass B3 MBLs, we determined the crystal structure of SMB-1, which has a broad-spectrum substrate specificity. We also obtained the SMB-1 structure complexed with MCR and demonstrated its mode of inhibition.

MATERIALS AND METHODS

Protein expression and purification. The expression of SMB-1 (GenBank accession no. AB636283) and its purification were performed according to previously described methods (15).

Crystallization. Crystallization of SMB-1 was performed as previously described (24). In brief, 3 μl of purified protein (15 mg/ml) and 3 μl of reservoir solution were mixed and equilibrated against 500 μl of reservoir solution at 293 K, using the hanging-drop vapor-diffusion method. Two types of crystals were prepared in the present study. One (native-1a) was obtained with the reservoir solution consisting of 0.2 M ammonium sulfate, 0.1 M sodium acetate trihydrate (pH 5.3), and 28% (wt/vol) PEG monomethyl ether (MME) 2000 (reservoir A). A second type of crystal (native-1b) was obtained using a reservoir solution consisting of 1 M lithium chloride, 0.1 M MES (morpholineethanesulfonic acid; pH 6.0), and 26% (wt/vol) PEG 6000 (reservoir B). Both crystals were grown within 1 week to a size suitable for collecting diffraction data. Crystals in a complex with MCR were obtained by soaking native-1b crystals in reservoir solutions containing 10 mM sodium MCR for 1 h.

Data collection and refinement. All diffraction data were collected at 100 K on a Beamline BL-5A at the Photon Factory (PF) and NW12A at the Photon Factory Advanced Ring (PF-AR) (High Energy Accelerator Research Organization, Tsukuba, Japan). The collected diffraction data were processed and scaled using the HKL-2000 program package (25).

The structure of native SMB-1 was initially solved using the data for the native-1a crystal by molecular replacement using the MOLREP program (26) in the CCP4 suite (27). The structure of L1 MBL that had been solved using 1.7-Å resolution diffraction data (PDB code 1SML) was modified by the deletion of water molecules, zinc ions, and several loop structures; mismatched amino acids were replaced with alanine. Molecular replacement was performed by using the modified L1 structure as the search model. The Coot program was used for model building (28), and the refinement was carried out using the REFMAC5 program (29), a component of the CCP4 suite (27).

The structures of native-1b and the SMB-1–MCR complex were solved by molecular replacement using the native structures determined from the crystal native-1a, and refined by the procedures described above. The quality of each finally refined model was assessed using the program PROCHECK (30) in the CCP4 suite (27). The data collection and refinement statistics are shown in Table 1.

Site-directed mutagenesis of bla_{SMB-1} and purification of mutant proteins. Site-directed mutagenesis was performed on the pCL-SMB plasmid (15), carrying the bla_{SMB-1} gene, with the Prime STAR mutagenesis basal kit (TaKaRa, Japan). Thereafter, the mutated gene was amplified by PCR, and the fragment was ligated into a pET30a vector (Novagen, Germany). Overexpression and purification of the mutant protein was performed according to a previously described method (15).

Kinetic parameters. The steady-state constants K_m and k_{cat} were determined according to a method described previously (15). The K_i value was determined using 100 μM nitrocefin as the reporter substrate.

TABLE 1 Data collection and refinement statistics[c]

Parameter	Native	Mercaptoacetate complex
Data collection		
Beam line	BL-5A (PF)	NW12A (PF-AR)
Wavelength (Å)	1.00	1.00
Resolution range (Å)	50.0–1.60 (1.63–1.60)	50.0–2.20 (2.24–2.20)
Space group	$P3_1$	$P3_1$
Cell dimensions (Å)		
a	67.83	67.03
b	67.83	67.03
c	48.67	46.79
No. of unique reflections	32,909 (1,654)	11,951 (621)
Redundancy	11.2	11.3
Completeness (%)	99.4 (100.0)	100.0 (100.0)
R_{merge}[a] (%)	5.1 (21.6)	9.7 (29.0)
Mean I/σ (I)	73.4 (17.3)	48.2 (15.6)
V_M[b] (Å^3 Da^{-1})	2.33	2.19
Solvent content (%)	47.3	43.8
Refinement		
Resolution (Å)	27.8–1.60 (1.64–1.60)	58.1–2.20 (2.26–2.20)
No. of reflections used	31,222 (2,313)	11,367 (873)
$R_{working}$ (%)	16.5 (21.0)	16.7 (16.4)
R_{free} (%)	20.0 (27.1)	22.4 (29.4)
No. of atoms		
Protein	1921	1907
Ligand/ion	53	9
Water	277	146
B-factors (Å^2)		
Protein	19.3	27.8
Ligand/ion	35.5	25.6
Water	31.3	29.6
RMSD		
Bond length (Å)	0.011	0.008
Bond angle (°)	1.43	1.18

[a] $R_{merge} = \sum_{hkl}\sum_i|I_i(hkl) - <I(hkl)>|/\sum_{hkl}\sum_i I_i(hkl)$, where $I_i(hkl)$ is the observed intensity for reflection for *hkl*, and $<I(hkl)>$ is the average intensity calculated for reflection *hkl* from replicate data.
[b] V_M, Matthews coefficient.
[c] Values in parentheses are for the highest-resolution shell.

Susceptibility testing. Susceptibility testing was performed according to Clinical and Laboratory Standards Institute (CLSI) guidelines (31).

Protein data bank accession numbers. The atomic coordinates and structural factors of native SMB-1 and the SMB-1-MCR complex have been deposited in the Protein Data Bank under accession numbers 3VPE and 3VQZ, respectively.

BBL and amino acid sequence numbers. The amino acid residues of SMB-1 were assigned with BBL and amino acid sequence numbers by putting the latter number in square brackets, e.g., "R37[3]," while those of MBLs other than SMB-1 were assigned with the BBL number only (32).

RESULTS AND DISCUSSION

Overall structure of SMB-1 and its complex with MCR. The MBL SMB-1 was crystallized using two different reservoir solutions (reservoirs A and B in Materials and Methods). Both crystals (native-1a and native-1b) diffracted to 1.6 Å and belonged to the trigonal space group $P3_1$, with one molecule per asymmetric unit. Both of the finally refined structures commonly contained the residues from R37[3] to K309[261] out of the matured SMB-1 (the 262 amino acids from Q35[1] to R310[262]) and two zinc ions with a full occupancy in the active site (Fig. 1). The superpo-

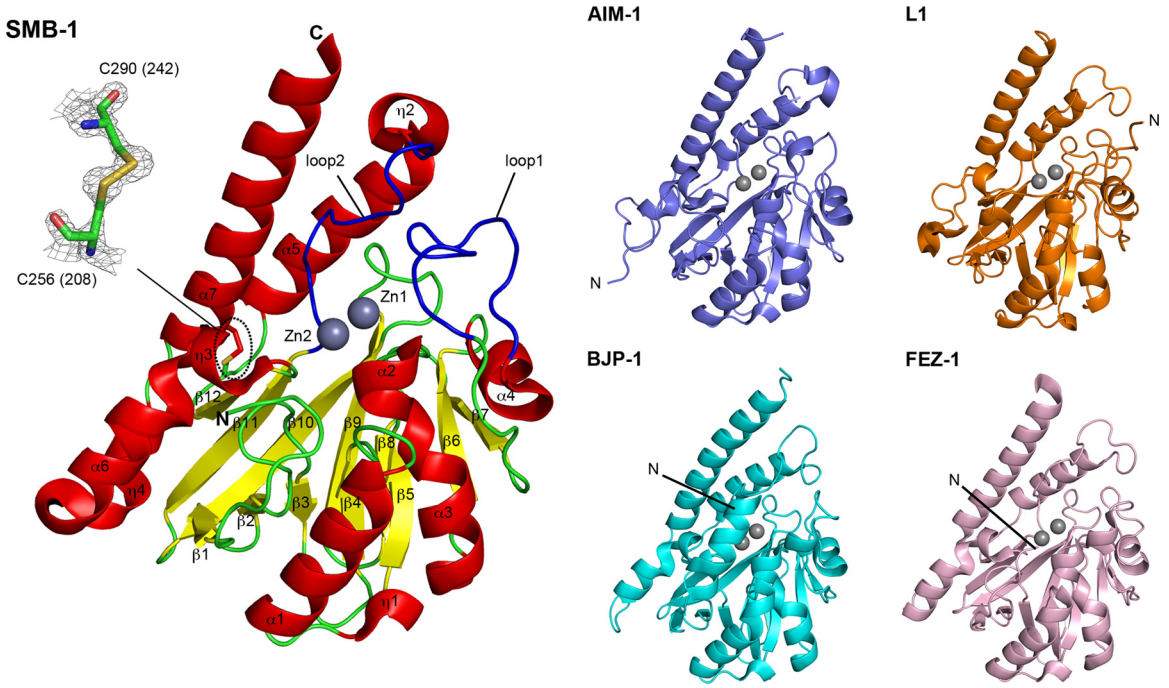

FIG 1 Schematic representation of the overall structure of SMB-1 and those of the other subclass B3 MBLs, AIM-1 (PDB code 4AWY, slate-blue), L1 (PDB code 1SML, orange), BJP-1 (PDB code 3LVZ, cyan), and FEZ-1 (PDB code 1K07, light pink). In the structure of SMB-1, the α-helices are shown in red, the β-strands are shown in yellow, and the loop region is shown in green. The two loops (loop1 and loop2) covering the active site are shown in blue. The two zinc ions are shown as gray spheres. The disulfide bond is circled with dashed lines and enlarged at the side. The figures were drawn with PyMOL.

sition of C^{α} atoms from the two native structures gave the root mean square deviation (RMSD) of 0.2 Å, indicating that the three-dimensional structures of two molecules are almost identical, with no substantial conformational differences. Unless otherwise noted, all subsequent descriptions referring to the native SMB-1 structure originate from the structure determined using the native-1a crystal data, because this yielded superior $R_{working}$ and R_{free} values of 0.17 and 0.20, respectively. A Ramachandran plot revealed that most of the residues (98.1%) are positioned in the favored region, and 1.9% residues are in the allowed region.

Next, we attempted to make SMB-1–MCR complex crystals by soaking the native crystals in reservoir solution containing sodium MCR. Diffraction data suitable for structural analysis were obtained only when soaking native-1b crystals, not native-1a crystals, despite repeated attempts. Similar to the native structure, SMB-1–MCR complex crystals belonged to the trigonal space group $P3_1$, with one molecule per asymmetric unit, and contained residues R37[3] to K309[261] and two zinc ions, as did the native structure, but with the exception of S160[116] and L161[117] (Fig. 2), which were disordered in the electron density map and were missing from the final model. The RMSD value between C^{α} atoms from the native SMB-1 and SMB-1–MCR complex was 0.3 Å, although the structure of the SMB-1–MCR complex was finally refined to 2.2 Å, which is lower than that of the native structure. The details of the data collection, crystallographic statistics of the structure determination, and refinements are shown in Table 1.

The overall structure of native SMB-1 is shown in Fig. 1. The SMB-1 structure contains 7 α-helices and 12 β-strands which form an αβ/βα sandwich structure, a common feature observed in β-lactam-hydrolyzing MBLs (33). The active site of SMB-1 was located at the bottom of a shallow cleft formed by the facing β-sheets; one sheet (N-terminal) consists of seven antiparallel strands (β1-β7), while the other (C-terminal) is composed of five antiparallel strands (β8-β12). The basis of the active site of SMB-1 was typically coordinated by two zinc ions (Zn1 and Zn2). Two loops connecting helix α4 and strand β7 (loop1), and strand β11 and helix α5 (loop2), which are typical features of subclass B3 MBLs, cover the center active-site cavity. A disulfide bridge is formed by residues C256[208] and C290[242] (Fig. 1), and the interaction pulled the last long helix α7 to the core domain of the protein. This disulfide bridge has also been observed in the other subclass B3 MBLs, AIM-1, L1, and FEZ-1, but not in BJP-1 (20, 34–36).

Coordination mode of active site. The active site in SMB-1 has two zinc ions (Zn1 and Zn2) separated by 3.5 Å (Fig. 3A). The zinc coordination mode of SMB-1 was similar to that of BJP-1 (34), whose structure was determined from high-resolution diffraction data (1.4 Å). Zn1 was coordinated to three histidine residues (H116[72], H118[74], and H196[150]) and the bridging hydroxide oxygen atom (Wat1) in a distorted tetrahedral geometry. Wat1 is assumed to contribute as the attacking nucleophile on the carbonyl carbon of the β-lactam ring. The bridging hydroxide anion is slightly asymmetrical with Zn-O distances being 2.0 and 2.1 Å for Zn1 and Zn2, respectively. The Zn1-Zn2 distance (3.5 Å) and the Zn1-OH^{-} (Wat1)-Zn2 angle (117°) are close to the corresponding distance (3.5 Å for subunit A and 3.4 Å for subunit B) and angle (119° for subunit A and 121° for subunit B) in BJP-1 (34). The Zn1-His distances are in the range of 2.0 to 2.1 Å (Table 2). The ranges of the His-Zn1-His and His-Zn1-O angles are 99° to 101° and 113° to 123°, respectively, and there is a significant distortion from the tetrahedral angle of 109.5°. This distortion may result from zinc ion d^{10} configuration due to the lack of ligand field stabilization.

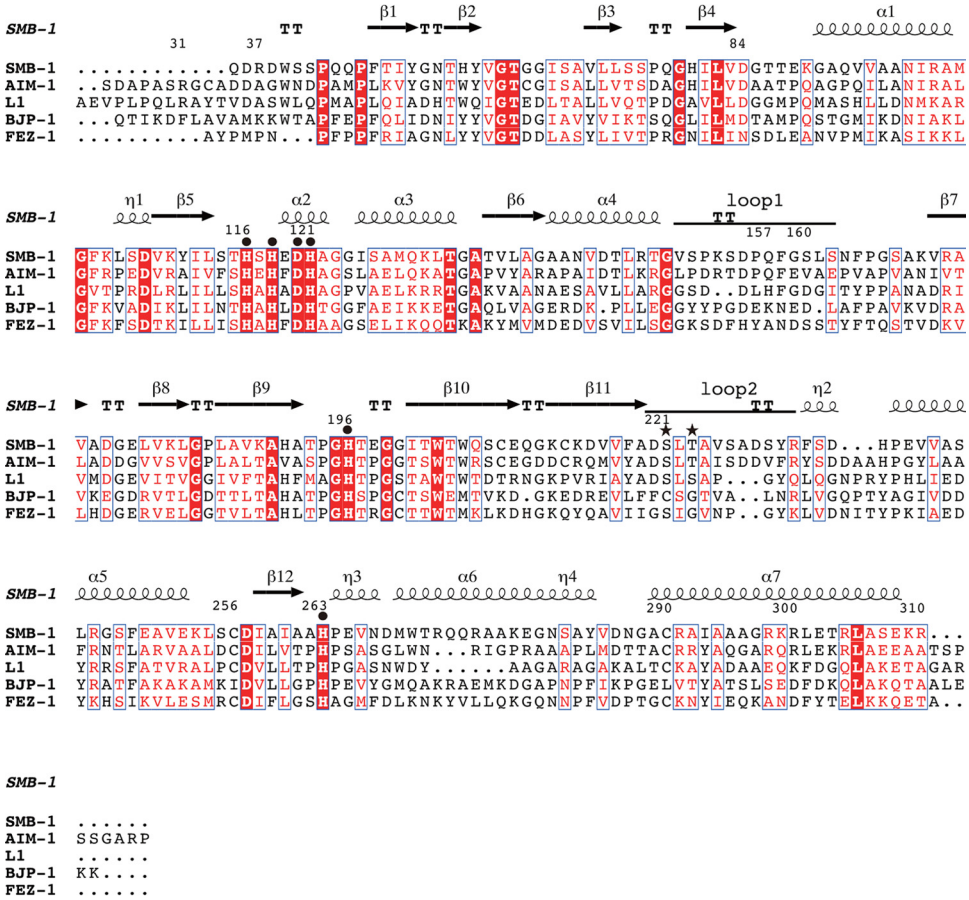

FIG 2 Amino acid alignment of the subclass B3 MBLs, SMB-1, AIM-1, L1, BJP-1, and FEZ-1 protein sequences. The strictly conserved amino acid residues are boxed in red. Physicochemically similar amino acids are shown in red. Closed circles indicate the amino acids involved in binding zinc ions. Stars indicate the residues binding to MCR. The secondary structure elements of SMB-1 are shown above the alignments. The figure was prepared using CLUSTAL W and ESPript.

In the Zn2 site, the geometry around Zn2 can be regarded as a distorted square pyramid with H263[215], D120[76], the bridging hydroxide oxygen atom (Wat1), and Wat2 on the equatorial base and H121[77] at the apex (Fig. 3A). The value of the stereochemical τ parameter (37), which could discriminate between a square pyramid (τ = 0) and trigonal bipyramid (τ = 1), is 0.37 {τ = [β-α]/60, where α = 144° for O (Wat1)-Zn2-H263[215] NE2 and β = 166° for O (Wat2)-Zn2-D120[76] OD2}. The Zn2-ligand distances are in the range of 2.1 to 2.2 Å, in which Wat2 is tightly bound to Zn2 (2.2 Å), compared to the corresponding distance (2.5 Å) in BJP-1 (34). It must be pointed out that one of the carboxylate oxygen atoms of D120[76] is also involved in hydrogen bonding to the bridging hydroxide oxygen atom (Wat1), suggesting that D120[76] may be particularly important not only in orientating an OH^- acting as a nucleophile to the carbonyl carbon on the β-lactam ring but also in positioning the Zn2 and H263[215], as seen also in the subclass B1 and B3 MBLs (38–40). These results suggested that SMB-1 has the ability to keep the coordination geometry closer to the transition state through distortion of the regular geometry.

Structural comparison with other subclass B3 MBLs. The structure of SMB-1 and those of other subclass B3 MBLs, *viz.*, AIM-1 (PDB code 4AWY), BJP-1 (PDB code 3LVZ), L1 (PDB code 1SML), and FEZ-1 (PDB code 1K07), which have 44, 28, 32, and 29% amino acid identities to SMB-1, respectively, were compared (Fig. 2). These five proteins shared very close protein folds, as reflected by RMSD values of 1.4 to 1.9 Å (Fig. 1). On the other hand, some remarkable structural differences were observed. The secondary structures of the N termini of SMB-1, AIM-1, and L1 consist of random coil, whereas BJP-1 has an α-helix in its N-terminus region (Fig. 1). The N-terminus region of SMB-1 was much shorter than those of the other subclass B3 MBLs, although the N-terminal regions aligned well from residue W39[5] in SMB-1, AIM-1, L1, and BJP-1. Site-directed mutagenesis approaches have previously revealed that the W39 residue could influence the recognition of β-lactams in subclass B3 MBLs (41). We propose that the difference in the structure of the N termini produces differences in the hydrolytic activity of subclass B3 MBLs, such that SMB-1, AIM-1, and L1 from human opportunistic pathogens have a higher catalytic efficiency (k_{cat}/K_m) against β-lactams, whereas FEZ-1 and BJP-1, derived from environmental bacteria, have relatively lower k_{cat}/K_m values (8, 15, 16, 18, 20).

Docquier et al. have shown that the low affinities exhibited by BJP-1 for various β-lactams could be attributed to the presence of amino acid residues, like F31, in the N-terminal helix, which results in a narrower space in the active site for the binding of the β-lactams, by occupying a space in which the R1 side chain of β-lactam is assumed to be primarily positioned (Fig. 1 and 4) (34).

On the other hand, the innate N-terminus region of SMB-1 is much shorter than that of BJP-1; this would make it possible to

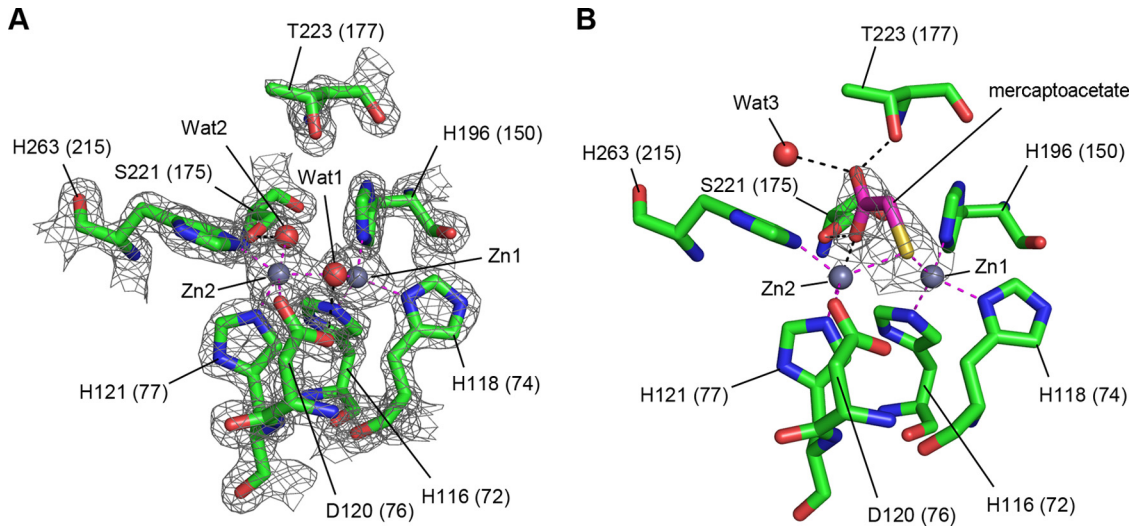

FIG 3 (A) Representation of the active site of native SMB-1. The zinc ions and water molecules are shown as gray and red spheres, respectively. The residues involved in the binding of the zinc ions are shown as green (carbon), blue (nitrogen), and red (oxygen) sticks. The electron density map (gray mesh) is shown countered at the 1.0σ level in the $2|Fo| - |Fc|$ map. The coordinate bonds around the zinc ions are shown as magenta dotted lines. The hydrogen bonds are shown as black dotted lines. (B) Representation of the active site of SMB-1 in complex with MCR. The MCR molecule is shown with magenta (carbon), yellow (sulfur), and red (oxygen) sticks. The zinc ions, zinc-binding residues, and the electron density map are shown with the color code used in panel A. The coordinate bonds around the zinc ions and the hydrogen bonds are shown as magenta and black dotted lines, respectively. The figures were drawn with PyMOL.

reserve a space for accommodating a wide range of β-lactams, even those with a bulky R1 side chain (Fig. 4). The broader substrate specificity observed in SMB-1 may thus partially depend on the space created by the loss of a long N-terminus structure that includes the residues interfering with substrate binding. AIM-1 and L1 have a long N-terminus structure similar to that of BJP-1, but their conformations and orientations largely differ from that of BJP-1 (Fig. 1). Both the N terminus of AIM-1 and that of L1 extend outward from the active site, avoiding narrowing of the space for substrate binding, and resulting in the creation of a space for accommodating β-lactams.

Structural comparison between subclass B3 MBLs, with a focus on the loop regions around the active site. The two loop regions (loop1 and loop2) were commonly considered to cover the active-site cavity in the subclass B3 MBLs (Fig. 5A). The two loops of SMB-1 adopt a very similar conformation to those of AIM-1, although loop2 in AIM-1 was partially disordered, but the conformation differed markedly compared to that of the other subclass B3 MBLs: L1, BJP-1, and FEZ-1. Loop1 (hairpin loop) and loop2 of SMB-1 and AIM-1 were spatially closer together than those of any other subclass B3 MBLs (Fig. 5A).

TABLE 2 Zinc(II)-ligand distances

Zn atom	Atom or molecule	Distance (Å)	
		Native	MCR complex
Zn1	H116[72] NE2	2.1	2.1
	H118[74] ND1	2.1	2.0
	H196[150] NE2	2.0	2.1
	O (Wat1)	2.0	
	O (Wat2)	3.1	
	O2 (MCR)		3.1
	S (MCR)		2.2
Zn2	D120[76] OD2	2.1	2.1
	H121[77] NE2	2.1	2.0
	H263[215] NE2	2.1	2.0
	O (Wat1)	2.1	
	O (Wat2)	2.2	
	S (MCR)		2.4
	O2 (MCR)		2.6
Zn1	Zn2	3.5	3.6

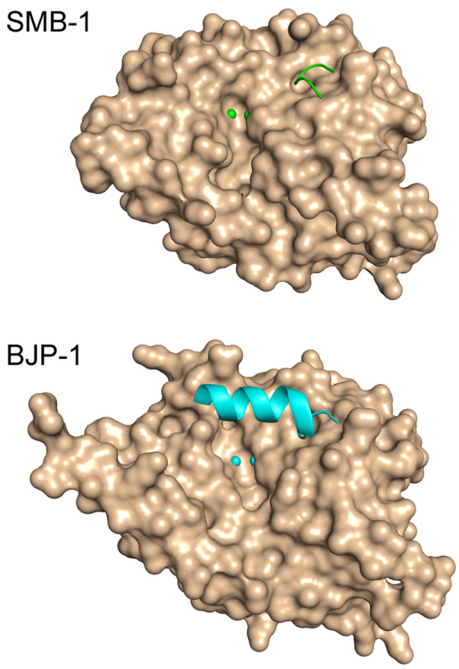

FIG 4 Molecular surface representations of SMB-1 and BJP-1. The N-terminal regions of SMB-1 and BJP-1 are shown as green and cyan secondary structures, respectively. The zinc ions in the active-site cavity are shown as spheres. The figures were drawn with PyMOL.

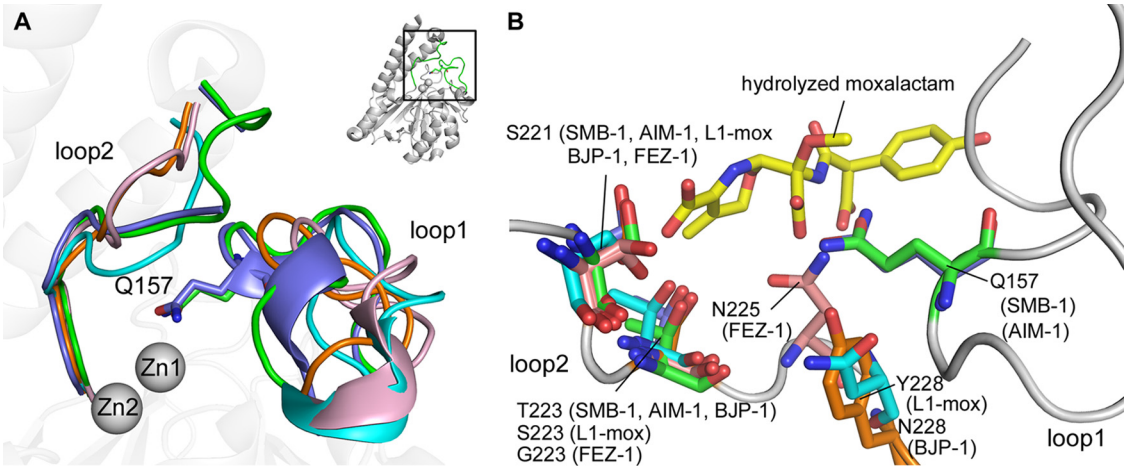

FIG 5 (A) Structural comparison of SMB-1 with AIM-1, L1, FEZ-1, and BJP-1, with particular focus on the two loop regions (loop1 and loop2). The overall structure of SMB-1 was drawn at right upper side. The part boxed with black lines in SMB-1 structure is enlarged and drawn with focus on the two loop regions. For SMB-1, the two loops are shown in green. The two zinc ions are shown as gray spheres. For AIM-1, L1, BJP-1, and FEZ-1, only the two loop regions are shown and are colored in slate blue, orange, cyan, and light pink, respectively. (B) Superposition of SMB-1 (green), AIM-1 (PDB code 4AWY; slate blue), L1-mox (PDB code 2AIO; orange), BJP-1 (PDB code 3LVZ, cyan), and FEZ-1 (PDB code 1K07, light pink) structures with focus on the residues, which are predicted to be involved in β-lactam recognition. The hydrolyzed moxalactam in the L1-mox structure is indicated with yellow sticks.

We hypothesized that various substrate preferences among the subclass B3 MBLs could be attributed to structural differences in the two loop regions. In fact, some of the amino acid residues in these two loop regions are already known to be responsible for binding to the substrate β-lactam antibiotics and/or inhibitor agents, as revealed by the complexed structures of BJP-1-4-nitrobenzenesulfonamide and L1-hydrolyzed moxalactam (34, 42) and also by site-directed mutagenesis approaches (41, 43).

In subclass B1 MBLs, the N233 residue was thought to play a role in β-lactam recognition, by facilitating creation of an oxyanion hole with the carbonyl oxygen of the β-lactam ring (44). In superposition of the SMB-1 structure with that of IMP-1, the tip of the Q157[113] residue in loop1 of SMB-1, whose amide side chain is located at 3.9 Å from Zn1, was positioned similarly to N233 of IMP-1. This suggests the possibility that the role of Q157[113] of SMB-1 corresponds to that of N233 of IMP-1. Q157[113] is a unique residue observed only in horizontally acquired subclass B3 MBLs, such as SMB-1 and AIM-1, but not in chromosomally encoded intrinsic subclass B3 MBLs, such as L1, BJP-1, and FEZ-1. Lerios et al. created an *in silico* docking model of an AIM-1-hydrolyzed cefoxitin structure and revealed the contacts between NE2 of Q157 and an oxygen of the C8 carboxylate group and also between NE2 of Q157 and a C10 carbonyl oxygen of hydrolyzed cefoxitin (20). Thus, the Q157[113] residue of SMB-1 would also contribute to the recognition of β-lactams, as it does in AIM-1. To elucidate the role of the Q157[113] residue in greater detail, we engineered a mutant in which the Q157[113] residue was replaced by an alanine; we established the steady-state kinetic constants of this molecule and tested its susceptibility. The Q157A[113] mutant protein showed increased K_m values for ampicillin, cefotaxime, ceftazidime, and imipenem, although the k_{cat} values for ampicillin and cefotaxime were somewhat increased (Table 3). In all, for the tested six β-lactams, the decrease in catalytic efficiency (k_{cat}/K_m) through alanine replacement at the Q157[113] residue was not large, which corresponded to the moderate reduction in MIC observed (Table 3). In the case of AIM-1, the replacement of residue 157 by alanine caused only a modest decrease in catalytic efficiency (k_{cat}/K_m) for a variety of β-lactams, which is consistent with the case of SMB-1 (20). Thus, Q157[113] is likely to be nonessential for hydrolytic activity of SMB-1 (also in AIM-1) but seems to play a role in enhanced hydrolytic activity for β-lactams compared to the other subclass B3 MBLs, probably by increasing the ability of enzyme to bind to substrate. Residues in other MBLs playing a role similar to that of Q157[113] in SMB-1 are postulated to be Y228 and N228 in L1 and BJP-1 and N225 in FEZ-1, but all of these are provided by the loop2 region (Fig. 5B).

TABLE 3 Kinetic parameters and result of susceptibility testing[a]

Substrate	β-Lactamase	K_m (μM)	k_{cat} (s^{-1})	k_{cat}/K_m ($M^{-1}\ s^{-1}$)	MIC (μg/ml)
Ampicillin	Wild	102	247	2.4×10^6	> 512
	Q157A	200	305	1.5×10^6	512
	Control	–	–	–	2
Ceftazidime	Wild	57	4.4	7.7×10^4	128
	Q157A	259	0.32	1.2×10^3	32
	Control	–	–	–	0.25
Cefotaxime	Wild	35	31	8.9×10^5	4
	Q157A	240	44	1.8×10^5	1
	Control	–	–	–	0.03
Cefepime	Wild	747	2.7	3.6×10^3	0.13
	Q157A	428	0.28	6.5×10^2	0.06
	Control	–	–	–	0.015
Imipenem	Wild	133	518	3.9×10^6	4
	Q157A	600	248	4.1×10^5	1
	Control	–	–	–	0.25
Meropenem	Wild	144	604	4.2×10^6	2
	Q157A	102	167	1.6×10^6	0.5
	Control	–	–	–	0.03

[a] The standard deviations for each parameter were below 20%. The data for the wild-type enzyme are from the reference 15. –, Not applicable.

In the structure of L1 with hydrolyzed moxalactam (PDB code 2AIO), interaction was observed between the S223 residue in loop2 and the C4 carboxylate group of hydrolyzed moxalactam (Fig. 5B). The T223[177] residue in SMB-1 was situated in the same position as the S223 residue in the L1 structure (Fig. 5B) and is likely to be involved in β-lactam substrate recognition. On the other hand, no such interaction was observed in the narrow-spectrum FEZ-1 due to the absence of a side chain at the G223 residue (Fig. 5B). The lower affinity of FEZ-1 for meropenem was also simulated in an *in silico* model by Liang et al. (45), which showed no such interactions, except for with the lactam motif. Although the main chain conformation surrounding the C4 carboxylate group differs little between subclass B3 MBLs, the slight difference in the position and orientation of side chains may influence the recognition of β-lactams.

Overall, it is likely that SMB-1 can accommodate a wider range of β-lactams by having more amino acid residues like Q157[113] around the active site, which are probably needed for recognition of the substrate β-lactams, than do BJP-1 and FEZ-1, subclass B3 MBLs with high K_m values for various β-lactams. This would explain the observed extended-spectrum activity of SMB-1 compared to BJP-1 and FEZ-1. Further structural analysis of SMB-1 in complex with various β-lactams would yield further insights into this proposal.

Binding mode of MCR in the active site. MCR is known as a reversible competitive inhibitor against the IMP-1 MBL, which belongs to subclass B1 (46). We determined the K_i value of SMB-1 for MCR to be 9.4 ± 0.4 μM, suggesting that MCR could behave as a potent inhibitor for SMB-1. Based on this finding, MCR was soaked into the SMB-1 crystal, and the complex structure was solved to 2.2 Å. In the SMB-1–MCR complexed structure, one MCR molecule was bound to the active site (Fig. 3B) to which β-lactams would originally bind. The thiolate group of MCR in the complexed structure replaced the bridging hydroxide anion (Wat1) between Zn1 and Zn2 observed in the native structure, where the thiolate group is bridged to two zinc ions (Zn1 and Zn2) with the distances of 2.2 Å for Zn1-S (MCR) and 2.4 Å for Zn2-S (MCR), respectively (Table 2). The Zn1-S (MCR) and Zn2-S (MCR) distances are close to those found in the D-captopril–L1 complex (2.3 and 2.2 Å) and the VIM-2–mercaptocarboxylate inhibitor complex (2.5 and 2.1 Å) (47, 48). Not only the thiolate group, but also the O2 atom of the carboxylate group in MCR is bound to Zn2 (2.6 Å), resulting in formation of a stable five-membered chelate ring (Fig. 3B); in most of the structures of MBLs complexed with compounds including a thiolate group determined thus far, only the thiolate group of the compound was coordinated to zinc ions (47–50).

In addition, the O2 atom of MCR forms a hydrogen bond to the hydroxyl OG of S221[175] (2.6 Å), and the O1 atom is involved in two hydrogen bonds with the hydroxyl OG1 of T223[177] (2.7 Å) and a water molecule (Wat3) (3.0 Å) (Fig. 3B). In the L1-hydrolyzed-moxalactam complexed structure (42), residues S221 and S223, which spatially correspond to S221[175] and T223[177] of SMB-1, were involved in the β-lactam recognition (Fig. 5B).

Furthermore, it is noteworthy that the binding of MCR to the active site causes a change in the coordination geometry of Zn2. The coordination around Zn1 in the complexed structure has a distorted tetrahedral geometry, which is similar to that in the native structure. On the other hand, the coordination around Zn2 in the complexed structure changed from a distorted square pyramid to a distorted trigonal bipyramid (Fig. 3B); the τ parameter was 0.83 {$\tau = [\beta-\alpha]/60$, where $\alpha = 120°$ for S (MCR)-Zn2-H263[215] NE2 and $\beta = 170°$ for O2 (MCR)-Zn2-D120[76] OD2}. Zn2 is located above 0.28 Å from the trigonal plane defined by H121[77] NE2, H263[215] NE2, and the thiolate group (S2) of MCR. The apical coordination sites are occupied by D120[76] OD2 and the carboxylate oxygen atom (O2) of MCR. The bond angle of O2 (MCR)-Zn2-D120[76] OD2 is 170° and the sum of the equatorial angles is 354°; 111° (H121[77] NE2-Zn2-H263[215] NE2), 123° (H121[77] NE2-Zn2-S2 (MCR)], and 120° (H263[215] NE2-Zn2-S2). The introduction of MCR yielded a slight increase (0.1 Å) in the distance between Zn1 and Zn2, compared to the native structure (Table 2). The structural observation of the binding mode of MCR to SMB-1 demonstrated that the mechanism of inhibition by MCR depended on the fact that the thiol group of MCR occupied the space, at which the hydroxide anion nucleophile (Wat1), which was assumed to contribute to the attacking on the carbonyl oxygen of the β-lactam ring, should originally locate.

Although a variety of the organic compounds, including a thiol group, have been designed and synthesized as MBL inhibitors, none have been used clinically (48, 51). Another possible use of these inhibitors is in development of a practical screening method for identification of MBL producers in the clinical microbiology setting (22, 23). The structure of the MCR complex presented here strongly suggests the potential and broad versatility of MCR as an MBL inhibitor. Thus, a screening approach employing MCR as an inhibitor would be universally applicable for identifying pathogenic bacteria that produce MBLs, including subclass B1 and B3 MBLs, as well as other MBLs that may emerge in future.

Conclusions. We report here the crystal structure of a subclass B3 MBL, SMB-1, and that of its complex with MCR. The higher catalytic efficiency against a wide range of β-lactams that was observed for SMB-1 could be attributed to the protein having a space capable of accommodating a wide range of β-lactams even with a bulky R1 side chain, provided by a loss of the long N terminus structure as observed in BJP-1, which includes residues such as F31 that prevent β-lactams from binding to the active site. Moreover, the presence of the amino acids such as Q157[113] provided by the loop regions would also contribute to recognition of β-lactams. Taken together, the difference in the accessibility of β-lactams to the active site and in the mode of β-lactam recognition by the residues from the two loop regions would influence the ability of the enzyme to recognize and catalyze β-lactams between subclass B3 MBLs, resulting in the major differences in the enzymatic behavior of subclass B3 MBLs.

In addition, through the inhibitor complexed structure, we could provide a rational model for the precise mode of inhibition of MCR on MBLs. MCR binds to the active site mainly by interaction with zinc ions, which is conserved in all of the MBLs found thus far. Therefore, a small MCR molecule would behave as a potent, universal inhibitor against MBLs, including subclass B1 and B3 MBLs. Moreover, MCR could be a powerful tool for screening for MBL-producing pathogenic bacteria in a clinical microbiology laboratory setting. Although commercially available serine–β-lactamase inhibitors, such as clavulanic acid, sulbactam, and tazobactam, are currently coadministered with antibiotic therapy, no MBL inhibitors have been marketed to date. The knowledge obtained from the structure presented here can shed

light on development of a potent inhibitor for MBLs, and may help in overcoming carbapenem resistance.

ACKNOWLEDGMENTS

This study was supported by grants from the Japanese Ministry of Education, Culture, Sports, Science, and Technology (Wakate B) and the Japanese Ministry of Health, Labor, and Welfare (H24-Shinkou-Ippan-010).

We are grateful to the staff of the Beamline BL-5A and NW12A at the Photon Factory (Tsukuba, Japan).

REFERENCES

1. **Nordmann P, Naas T, Poirel L.** 2011. Global spread of carbapenemase-producing *Enterobacteriaceae*. Emerg. Infect. Dis. **17**:1791–1798.
2. **Galleni M, Lamotte-Brasseur J, Rossolini GM, Spencer J, Dideberg O, Frere JM.** 2001. Standard numbering scheme for class B β-lactamases. Antimicrob. Agents Chemother. **45**:660–663.
3. **Walsh TR, Hall L, Assinder SJ, Nichols WW, Cartwright SJ, MacGowan AP, Bennett PM.** 1994. Sequence analysis of the L1 metallo-β-lactamase from *Xanthomonas maltophilia*. Biochim. Biophys. Acta **1218**:199–201.
4. **Bellais S, Leotard S, Poirel L, Naas T, Nordmann P.** 1999. Molecular characterization of a carbapenem-hydrolyzing β-lactamase from *Chryseobacterium* (*Flavobacterium*) *indologenes*. FEMS Microbiol. Lett. **171**:127–132.
5. **Saavedra MJ, Peixe L, Sousa JC, Henriques I, Alves A, Correia A.** 2003. Sfh-I, a subclass B2 metallo-β-lactamase from a *Serratia fonticola* environmental isolate. Antimicrob. Agents Chemother. **47**:2330–2333.
6. **Rasmussen BA, Gluzman Y, Tally FP.** 1990. Cloning and sequencing of the class B β-lactamase gene (*ccrA*) from *Bacteroides fragilis* TAL3636. Antimicrob. Agents Chemother. **34**:1590–1592.
7. **Docquier JD, Pantanella F, Giuliani F, Thaller MC, Amicosante G, Galleni M, Frere JM, Bush K, Rossolini GM.** 2002. CAU-1, a subclass B3 metallo-β-lactamase of low substrate affinity encoded by an ortholog present in the *Caulobacter crescentus* chromosome. Antimicrob. Agents Chemother. **46**:1823–1830.
8. **Stoczko M, Frere JM, Rossolini GM, Docquier JD.** 2006. Postgenomic scan of metallo-β-lactamase homologues in rhizobacteria: identification and characterization of BJP-1, a subclass B3 ortholog from *Bradyrhizobium japonicum*. Antimicrob. Agents Chemother. **50**:1973–1981.
9. **Osano E, Arakawa Y, Wacharotayankun R, Ohta M, Horii T, Ito H, Yoshimura F, Kato N.** 1994. Molecular characterization of an enterobacterial metallo β-lactamase found in a clinical isolate of *Serratia marcescens* that shows imipenem resistance. Antimicrob. Agents Chemother. **38**:71–78.
10. **Lauretti L, Riccio ML, Mazzariol A, Cornaglia G, Amicosante G, Fontana R, Rossolini GM.** 1999. Cloning and characterization of bla_{VIM}, a new integron-borne metallo-β-lactamase gene from a *Pseudomonas aeruginosa* clinical isolate. Antimicrob. Agents Chemother. **43**:1584–1590.
11. **Yong D, Toleman MA, Giske CG, Cho HS, Sundman K, Lee K, Walsh TR.** 2009. Characterization of a new metallo-β-lactamase gene, bla_{NDM-1}, and a novel erythromycin esterase gene carried on a unique genetic structure in *Klebsiella pneumoniae* sequence type 14 from India. Antimicrob. Agents Chemother. **53**:5046–5054.
12. **Toleman MA, Simm AM, Murphy TA, Gales AC, Biedenbach DJ, Jones RN, Walsh TR.** 2002. Molecular characterization of SPM-1, a novel metallo-β-lactamase isolated in Latin America: report from the SENTRY antimicrobial surveillance programme. J. Antimicrob. Chemother. **50**:673–679.
13. **Castanheira M, Toleman MA, Jones RN, Schmidt FJ, Walsh TR.** 2004. Molecular characterization of a β-lactamase gene, bla_{GIM-1}, encoding a new subclass of metallo-β-lactamase. Antimicrob. Agents Chemother. **48**:4654–4661.
14. **Lee K, Yum JH, Yong D, Lee HM, Kim HD, Docquier JD, Rossolini GM, Chong Y.** 2005. Novel acquired metallo-β-lactamase gene, bla_{SIM-1}, in a class 1 integron from *Acinetobacter baumannii* clinical isolates from Korea. Antimicrob. Agents Chemother. **49**:4485–4491.
15. **Wachino J, Yoshida H, Yamane K, Suzuki S, Matsui M, Yamagishi T, Tsutsui A, Konda T, Shibayama K, Arakawa Y.** 2011. SMB-1, a novel subclass B3 metallo-β-lactamase, associated with IS*CR1* and a class 1 integron, from a carbapenem-resistant *Serratia marcescens* clinical isolate. Antimicrob. Agents Chemother. **55**:5143–5149.
16. **Crowder MW, Walsh TR, Banovic L, Pettit M, Spencer J.** 1998. Overexpression, purification, and characterization of the cloned metallo-β-lactamase L1 from *Stenotrophomonas maltophilia*. Antimicrob. Agents Chemother. **42**:921–926.
17. **Horsfall LE, Izougarhane Y, Lassaux P, Selevsek N, Lienard BM, Poirel L, Kupper MB, Hoffmann KM, Frere JM, Galleni M, Bebrone C.** 2011. Broad antibiotic resistance profile of the subclass B3 metallo-β-lactamase GOB-1, a di-zinc enzyme. FEBS. J. **278**:1252–1263.
18. **Mercuri PS, Bouillenne F, Boschi L, Lamotte-Brasseur J, Amicosante G, Devreese B, van Beeumen J, Frere JM, Rossolini GM, Galleni M.** 2001. Biochemical characterization of the FEZ-1 metallo-β-lactamase of *Legionella gormanii* ATCC 33297T produced in *Escherichia coli*. Antimicrob. Agents Chemother. **45**:1254–1262.
19. **Rossolini GM, Condemi MA, Pantanella F, Docquier JD, Amicosante G, Thaller MC.** 2001. Metallo-β-lactamase producers in environmental microbiota: new molecular class B enzyme in *Janthinobacterium lividum*. Antimicrob. Agents Chemother. **45**:837–844.
20. **Leiros HK, Borra PS, Brandsdal BO, Edvardsen KS, Spencer J, Walsh TR, Samuelsen O.** 2012. Crystal structure of the mobile metallo-β-lactamase AIM-1 from *Pseudomonas aeruginosa*: insights into antibiotic binding and the role of Gln157. Antimicrob. Agents Chemother. **56**:4341–4353.
21. **Toleman MA, Bennett PM, Walsh TR.** 2006. ISCR elements: novel gene-capturing systems of the 21st century? Microbiol. Mol. Biol. Rev. **70**:296–316.
22. **Shibata N, Doi Y, Yamane K, Yagi T, Kurokawa H, Shibayama K, Kato H, Kai K, Arakawa Y.** 2003. PCR typing of genetic determinants for metallo-β-lactamases and integrases carried by gram-negative bacteria isolated in Japan, with focus on the class 3 integron. J. Clin. Microbiol. **41**:5407–5413.
23. **Tsutsui A, Suzuki S, Yamane K, Matsui M, Konda T, Marui E, Takahashi K, Arakawa Y.** 2011. Genotypes and infection sites in an outbreak of multidrug-resistant *Pseudomonas aeruginosa*. J. Hosp. Infect. **78**:317–322.
24. **Wachino J, Yamaguchi Y, Mori S, Yamagata Y, Arakawa Y, Shibayama K.** 2011. Crystallization and preliminary X-ray analysis of the subclass B3 metallo-β-lactamase SMB-1 that confers carbapenem resistance. Acta Crystallogr. Sect. F Struct. Biol. Crystallogr. Commun. **68**:343–346.
25. **Otwinowski Z, Minor W.** 1997. Processing of X-ray diffraction data collected in oscillation mode. Methods Enzymol. **276**:307–326.
26. **Vagin A, Teplyakov A.** 2010. Molecular replacement with MOLREP. Acta Crystallogr. D Biol. Crystallogr. **66**:22–25.
27. **Dodson EJ, Winn M, Ralph A.** 1997. Collaborative Computational Project, number 4: providing programs for protein crystallography. Methods Enzymol. **277**:620–633.
28. **Emsley P, Cowtan K.** 2004. Coot: model-building tools for molecular graphics. Acta Crystallogr. D Biol. Crystallogr. **60**:2126–2132.
29. **Murshudov GN, Vagin AA, Dodson EJ.** 1997. Refinement of macromolecular structures by the maximum-likelihood method. Acta Crystallogr. D Biol. Crystallogr. **53**:240–255.
30. **Lovell SC, Davis IW, Arendall WB III, de Bakker PI, Word JM, Prisant MG, Richardson JS, Richardson DC.** 2003. Structure validation by Cα geometry: ϕ,ψ and Cβ deviation. Proteins **50**:437–450.
31. **Clinical and Laboratory Standards Institute.** 2009. Methods for dilution antimicrobial susceptibility tests for bacteria that grow aerobically. Approved standard, 8th ed. Document M07-A8. CLSI, Wayne, PA.
32. **Garau G, Garcia-Saez I, Bebrone C, Anne C, Mercuri P, Galleni M, Frere JM, Dideberg O.** 2004. Update of the standard numbering scheme for class B β-lactamases. Antimicrob. Agents Chemother. **48**:2347–2349.
33. **Carfi A, Pares S, Duee E, Galleni M, Duez C, Frere JM, Dideberg O.** 1995. The 3-D structure of a zinc metallo-β-lactamase from *Bacillus cereus* reveals a new type of protein fold. EMBO J. **14**:4914–4921.
34. **Docquier JD, Benvenuti M, Calderone V, Stoczko M, Menciassi N, Rossolini GM, Mangani S.** 2010. High-resolution crystal structure of the subclass B3 metallo-β-lactamase BJP-1: rational basis for substrate specificity and interaction with sulfonamides. Antimicrob. Agents Chemother. **54**:4343–4351.
35. **Garcia-Saez I, Mercuri PS, Papamicael C, Kahn R, Frere JM, Galleni M, Rossolini GM, Dideberg O.** 2003. Three-dimensional structure of FEZ-1, a monomeric subclass B3 metallo-β-lactamase from *Fluoribacter gormanii*, in native form and in complex with D-captopril. J. Mol. Biol. **325**:651–660.
36. **Ullah JH, Walsh TR, Taylor IA, Emery DC, Verma CS, Gamblin SJ, Spencer J.** 1998. The crystal structure of the L1 metallo-β-lactamase from

Stenotrophomonas maltophilia at 1.7 Å resolution. J. Mol. Biol. **284**:125–136.
37. **Addison AW, Rao TN, Reedijk J, Rijn J, Verschoor GC.** 1984. Synthesis, structure, and spectroscopic properties of copper(II) compounds containing nitrogen–sulphur donor ligands; the crystal and molecular structure of aqua[1,7-bis(*N*-methylbenzimidazol-2′-yl)-2,6-dithiaheptane]copper(II) perchlorate. J. Chem. Soc. Dalton Trans. **7**:1349–1356.
38. **Crisp J, Conners R, Garrity JD, Carenbauer AL, Crowder MW, Spencer J.** 2007. Structural basis for the role of Asp-120 in metallo-β-lactamases. Biochemistry **46**:10664–10674.
39. **Llarrull LI, Fabiane SM, Kowalski JM, Bennett B, Sutton BJ, Vila AJ.** 2007. Asp-120 locates Zn2 for optimal metallo-β-lactamase activity. J. Biol. Chem. **282**:18276–18285.
40. **Yamaguchi Y, Kuroki T, Yasuzawa H, Higashi T, Jin W, Kawanami A, Yamagata Y, Arakawa Y, Goto M, Kurosaki H.** 2005. Probing the role of Asp-120(81) of metallo-β-lactamase (IMP-1) by site-directed mutagenesis, kinetic studies, and X-ray crystallography. J. Biol. Chem. **280**:20824–20832.
41. **Garrity JD, Pauff JM, Crowder MW.** 2004. Probing the dynamics of a mobile loop above the active site of L1, a metallo-β-lactamase from *Stenotrophomonas maltophilia*, via site-directed mutagenesis and stopped-flow fluorescence spectroscopy. J. Biol. Chem. **279**:39663–39670.
42. **Spencer J, Read J, Sessions RB, Howell S, Blackburn GM, Gamblin SJ.** 2005. Antibiotic recognition by binuclear metallo-β-lactamases revealed by X-ray crystallography. J. Am. Chem. Soc. **127**:14439–14444.
43. **Mercuri PS, Garcia-Saez I, De Vriendt K, Thamm I, Devreese B, Van Beeumen J, Dideberg O, Rossolini GM, Frere JM, Galleni M.** 2004. Probing the specificity of the subclass B3 FEZ-1 metallo-β-lactamase by site-directed mutagenesis. J. Biol. Chem. **279**:33630–33638.
44. **Concha NO, Rasmussen BA, Bush K, Herzberg O.** 1996. Crystal structure of the wide-spectrum binuclear zinc β-lactamase from *Bacteroides fragilis*. Structure **4**:823–836.
45. **Liang Z, Li L, Wang Y, Chen L, Kong X, Hong Y, Lan L, Zheng M, Guang-Yang C, Liu H, Shen X, Luo C, Li KK, Chen K, Jiang H.** 2011. Molecular basis of NDM-1, a new antibiotic resistance determinant. PLoS One **6**:e23606. doi:10.1371/journal.pone.0023606.
46. **Goto M, Takahashi T, Yamashita F, Koreeda A, Mori H, Ohta M, Arakawa Y.** 1997. Inhibition of the metallo-β-lactamase produced from *Serratia marcescens* by thiol compounds. Biol. Pharm. Bull. **20**:1136–1140.
47. **Nauton L, Kahn R, Garau G, Hernandez JF, Dideberg O.** 2008. Structural insights into the design of inhibitors for the L1 metallo-β-lactamase from *Stenotrophomonas maltophilia*. J. Mol. Biol. **375**:257–269.
48. **Yamaguchi Y, Jin W, Matsunaga K, Ikemizu S, Yamagata Y, Wachino J, Shibata N, Arakawa Y, Kurosaki H.** 2007. Crystallographic investigation of the inhibition mode of a VIM-2 metallo-β-lactamase from *Pseudomonas aeruginosa* by a mercaptocarboxylate inhibitor. J. Med. Chem. **50**:6647–6653.
49. **Kurosaki H, Yamaguchi Y, Higashi T, Soga K, Matsueda S, Yumoto H, Misumi S, Yamagata Y, Arakawa Y, Goto M.** 2005. Irreversible inhibition of metallo-β-lactamase (IMP-1) by 3-(3-mercaptopropionylsulfanyl)propionic acid pentafluorophenyl ester. Angew. Chem. Int. Ed. Engl. **44**:3861–3864.
50. **Lassaux P, Hamel M, Gulea M, Delbruck H, Mercuri PS, Horsfall L, Dehareng D, Kupper M, Frere JM, Hoffmann K, Galleni M, Bebrone C.** 2010. Mercaptophosphonate compounds as broad-spectrum inhibitors of the metallo-β-lactamases. J. Med. Chem. **53**:4862–4876.
51. **Lienard BM, Garau G, Horsfall L, Karsisiotis AI, Damblon C, Lassaux P, Papamicael C, Roberts GC, Galleni M, Dideberg O, Frere JM, Schofield CJ.** 2008. Structural basis for the broad-spectrum inhibition of metallo-β-lactamases by thiols. Org. Biomol. Chem. **6**:2282–2294.